IgA potentiates NETosis in response to viral infection

Hannah D. Stacey[a,b,c], Diana Golubeva[a,b,c], Alyssa Posca[a,b,c], Jann C. Ang[a,b,c], Kyle E. Novakowski[a,b,d], Muhammad Atif Zahoor[b,d,1], Charu Kaushic[b,d], Ewa Cairns[e,f], Dawn M. E. Bowdish[a,b,d], Caitlin E. Mullarkey[a], and Matthew S. Miller[a,b,c,2]

[a]Michael G. DeGroote Institute for Infectious Diseases Research, McMaster University, Hamilton, ON, Canada, L8S 4K1; [b]McMaster Immunology Research Centre, McMaster University, Hamilton, ON, Canada, L8S 4K1; [c]Department of Biochemistry and Biomedical Sciences, McMaster University, Hamilton, ON, Canada, L8S 4K1; [d]Department of Medicine, McMaster University, Hamilton, ON, Canada, L8S 4K1; [e]Department of Microbiology and Immunology, Schulich School of Medicine and Dentistry, Western University, London, ON, Canada, N6A 3K7; and [f]Department of Medicine, Division of Rheumatology, Schulich School of Medicine and Dentistry, Western University, London, ON, Canada, N6A 3K7

IgA is the second most abundant antibody present in circulation and is enriched at mucosal surfaces. As such, IgA plays a key role in protection against a variety of mucosal pathogens including viruses. In addition to neutralizing viruses directly, IgA can also stimulate Fc-dependent effector functions via engagement of Fc alpha receptors (Fc-αRI) expressed on the surface of certain immune effector cells. Neutrophils are the most abundant leukocyte, express Fc-αRI, and are often the first to respond to sites of injury and infection. Here, we describe a function for IgA–virus immune complexes (ICs) during viral infections. We show that IgA–virus ICs potentiate NETosis—the programmed cell-death pathway through which neutrophils release neutrophil extracellular traps (NETs). Mechanistically, IgA–virus ICs potentiated a suicidal NETosis pathway via engagement of Fc-αRI on neutrophils through a toll-like receptor–independent, NADPH oxidase complex–dependent pathway. NETs also were capable of trapping and inactivating viruses, consistent with an antiviral function.

NETosis | viruses | influenza | SARS-CoV-2 | neutrophils

IgA antibodies have pleiotropic roles in regulating the response to microbes. In the context of infection, IgA antibodies enriched at mucosal surfaces as secretory IgA (sIgA) are capable of neutralizing viruses in an "anti-inflammatory" manner, since these antibodies block infection but do not activate immune cells via Fc-receptor engagement. However, monomeric IgA (mIgA) antibodies, which are abundant in serum, are capable of engaging Fc receptors on the surface of immune cells to elicit effector functions (1).

Neutrophils are not only the most abundant leukocytes but are often the first to respond to sites of injury and infection (2). Human neutrophils express the Fc alpha receptor (Fc-αRI/CD89) and are capable of exerting a variety of effector functions including phagocytosis, respiratory burst, antibody-dependent cellular phagocytosis (ADCP), and NETosis (3, 4). Data regarding the protective versus pathogenic role of neutrophils during viral infection is nuanced and suggests context is critical in determining outcome. For example, while neutrophils are required for protection during the early stages of influenza A virus (IAV) infection, neutrophils also release reactive oxygen species (ROS), proteolytic enzymes, and a variety of inflammatory mediators that can damage lung tissues. As a result, excessive neutrophil infiltration has been associated with severe lung injury (5).

The generation of neutrophil extracellular traps (NETs) was first described by the Zychlinsky laboratory in 2004 as an antibacterial effector mechanism (6). NETs are produced via a specialized form of programmed cell death called NETosis and are composed primarily of decondensed chromatin studded with antimicrobial proteins. Extensive work by many laboratories has since demonstrated that NETs can have not only protective but also pathogenic consequences in infections and many other diseases (4). The understanding of how NETs influence viral infections continues to evolve. In the context of Chikungunya virus and poxvirus, NETs were capable of trapping viruses and controlling infection in a mouse model of disease (7, 8). Likewise, NETs have

been shown to trap and inactivate HIV (9). However, NETs have also been described as exacerbating disease in the context of Dengue virus, rhinovirus, respiratory syncytial virus, influenza virus, and, most recently, SARS-CoV-2 infection (10–16). Thus, the overall impact of NETs during a viral infection must be interpreted carefully in conjunction with other infection parameters.

Recently, Fc-dependent effector functions have been shown to play a central role in the protection conferred by broadly neutralizing antibodies (bnAbs) that bind to the hemagglutinin (HA) stalk domain of IAV (17–19). However, these studies have only been performed in the context of monoclonal IgG antibodies. Elicitation of bnAbs is now the goal of several "universal" influenza-virus vaccine candidates including "chimeric" HA vaccines that were recently tested in a Phase-I clinical trial (20). Antibody-dependent cellular cytotoxicity (ADCC) may also augment protection mediated by HIV-neutralizing antibodies (21). However, despite the fact that both IAV and HIV are mucosal pathogens, almost nothing is known about the contribution of IgA-mediated Fc-dependent effector functions during infection. This is due, in large part, to the fact that mice do not express an Fc-αR homolog, which presents significant challenges for assessing the contributions of IgA to outcomes in vivo (1).

Significance

IgA antibodies are enriched at mucosal surfaces and play an important role in host defense against viral pathogens. In addition to neutralizing viruses directly, antibodies can also engage specific receptors (Fc receptors) expressed on various immune-cell subsets to stimulate antimicrobial activities. While IgG Fc-mediated effector functions are known to mediate important antiviral activities, if and how IgA-mediated Fc-effector functions influence viral infections remains poorly understood. Here, we show that IgA–virus immune complexes stimulate neutrophils to undergo NETosis, a specific type of programmed cell death that results in release of chromatin studded with antimicrobial effector proteins. These neutrophil extracellular traps trap and inactivate viruses but can also have pathogenic consequences when poorly regulated.

MICROBIOLOGY

Here, we show that IgA–virus immune complexes (ICs) potentiated NETosis through Fc-αRI signaling on neutrophils. This potentiation was not virus specific and could be observed for IAV, HIV, and SARS-CoV-2 spike-pseudotyped lentiviruses and extended to IgA ICs generated with antibodies/autoantigens from rheumatoid arthritis (RA) patients. In contrast to NETosis stimulated by viruses directly, IgA–virus ICs stimulated suicidal NETosis that was independent of toll-like receptor (TLR) signaling. Finally, viruses were trapped and inactivated in NETs, suggesting a protective role in vivo when properly regulated.

Results

IgA–IAV ICs Stimulate NETosis. Historically, antibodies have been thought to mediate protection against influenza viruses primarily by binding to the HA head domain and blocking interaction between the receptor binding site on HA and sialic acids on the surface of host cells. However, more recently, it has become clear that bnAbs that bind to the HA stalk domain mediate protection in vivo primarily by elicitation of Fc-dependent effector functions (17–19). Antigen-specific IgA antibodies have been shown to

neutralize IAV, but relatively little is known about IgA-mediated Fc-dependent effector functions during IAV infection (22). Neutrophils are the most abundant leukocyte and are among the first to respond during IAV infection (23). Neutrophils also express FcαRI, and we have previously shown that IgA–IAV ICs stimulate ROS production in neutrophils; however, unlike IgG–influenza virus ICs, this could not be fully inhibited by cytochalasin D, indicating that IgA-mediated ROS production was not due to ADCP (24). To determine whether IgA was capable of potentiating NETosis upon binding IAV, neutrophils were exposed to antibody–IAV ICs composed of polyclonal (monomeric) IgA or IgG from the peripheral blood of donors previously vaccinated with seasonal influenza vaccines containing the A/California/04/2009 (Cal/09) H1N1 component. Phorbol 12-myrisate13-acetate (PMA), a potent inducer of NETosis, was used as a positive control (25). IgA–IAV ICs stimulated significantly higher levels of NETosis than antibodies or viruses alone, whereas IgG–IAV ICs did not induce NETosis above background levels (Fig. 1 A and B). A 2:1 ratio of IgA to virus reliably induced NETosis above background levels, while IgA-to-virus ratios of up to 10:1 did not
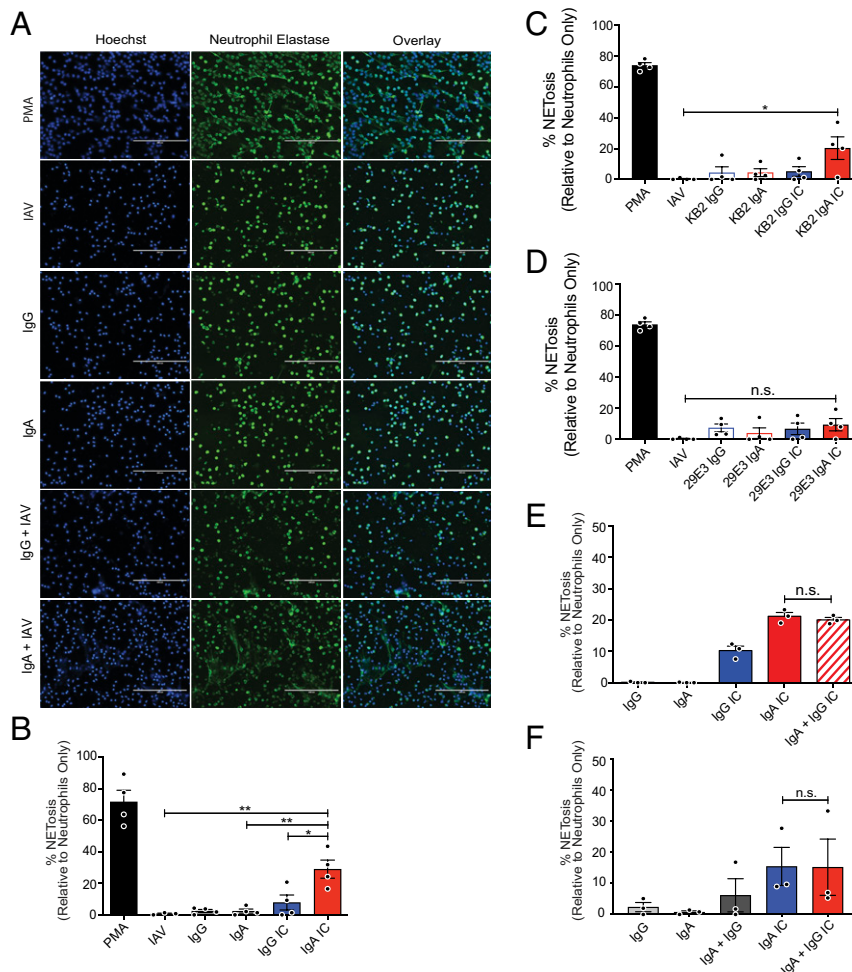

Fig. 1. IgA–IAV ICs potentiate NETosis. (A–F) Primary human neutrophils were isolated from the peripheral blood of healthy donors (n = 3 or 4) and stimulated with PMA, monoclonal or polyclonal IgG or IgA antibodies, or ICs for 3 h as shown. NETosis was assessed by immunofluorescence microscopy after costaining for DNA (Hoechst) and neutrophil elastase. (A) Representative images are shown (20×). (Scale bars, 200 μm.) (B) The percentage of cells that had undergone NETosis (defined by typically NET morphology and costaining of DAPI + neutrophil elastase) was quantified in a blinded manner from five fields in four independent experiments. (C and D) The assay was repeated using monoclonal antibodies, (C) KB2 and (D) 29E3, which bind the HA stalk and head domain of Cal/09, respectively. (E and F) To determine the phenotype of mixed IgG/IgA ICs, polyclonal IgG and IgA were mixed with Cal/09 at (E) a 1:1 ratio or (F) at the ratio naturally found in serum. For all experiments, percent NETosis was normalized to unstimulated neutrophils. Three or four independent neutrophil donors were used for each experiment. Means and SE (SEM) of independent experiments are shown. Statistical significance was determined using one-way ANOVA with Tukey post hoc test. *$P < 0.05$; **$P < 0.01$.

significantly further increase NETosis induction (*SI Appendix*, Fig. S1*A*).

In the context of IgG, bnAbs that bind to the stalk domain have been shown to potently elicit Fc-dependent effector functions, whereas antibodies that bind to the HA head domain and exhibit hemagglutination inhibiting activity do not. This is because HA stalk-binding bnAbs allow for two points of contact between target and effector cells (26, 27). To determine whether broadly neutralizing IgA–IAV ICs are primarily responsible for the induction of NETosis observed in the context of IAV-specific polyclonal IgA, we used a panel of previously described monoclonal antibodies that bind to neutralizing epitopes on either the HA head or stalk domains (28–30). The antibody KB2 binds to the HA stalk domain of H1 viruses, while 29E3 is specific to the HA head domain of Cal/09 (31). When human neutrophils were incubated with ICs containing an IAV–IgA1 stalk-binding antibody (KB2), significant induction of NETosis was observed following 3-h stimulation (Fig. 1*C*). In contrast, NETosis was not induced by IgG1–IAV ICs or by antibodies or viruses alone (Fig. 1*C*). We have previously shown that, under these conditions, IgG–IAV ICs potently induce neutrophil ADCP via FcγR signaling (24). As we had observed in the context of ADCP, all ICs generated with an HA head-binding antibody (29E3) failed to induce NETosis (Fig. 1*D*).

In blood, IgA cocirculates with other antibodies, including IgG, which signals through distinct FcRs (FcγRs) and can also induce NETosis (32). Mixed ICs composed of IgG/IgA–HIV have also been shown to act cooperatively to stimulate ADCC by monocytes (33). We therefore tested whether mixed ICs composed of IAV bound by IgA and IgG together would influence the magnitude of NETosis induction relative to IgA alone. When ICs were generated with a 1:1 ratio of IgG to IgA, the magnitude of NETosis induction was similar to IgA alone (Fig. 1*E*). In serum, IgG is significantly more abundant than IgA (~4:1 to 10:1). Thus, to recapitulate the physiological stoichiometry of IgG–IgA, we purified each immunoglobulin from serum of matched donors and then recombined them at their natural physiological ratio. Here again, the magnitude of NETosis observed in mixed IgG–IgA ICs was similar to IgA alone, indicating that IgG does not potentiate IgA-mediated NETosis, nor does it interfere with the ability of IgA to stimulate NETosis (Fig. 1*F*). Taken together, these results demonstrate that IgA–virus ICs stimulate neutrophils to undergo NETosis.

IgA-Mediated NETosis Is Not an IAV-Specific Phenomenon. NETs have been observed in the context of many other infections including those caused by COVID-19 and HIV. In these studies, viruses were presumed to stimulate NETosis directly (14, 16, 34, 35). We thus performed an experiment to test the amount of viruses needed to stimulate NETosis independent of FcαR signaling. Neutrophils were stimulated with increasing concentrations of purified lentiviruses pseudotyped with the SARS-CoV-2 spike protein. A significant elevation in NETosis was observed when neutrophils were exposed to 0.05 and 0.2 mg/mL purified virus (Fig. 2*A*). We then purified IgA from convalescence serum of a SARS-CoV-2–infected individual and a SARS-CoV-2–naïve individual, incubated them with substimulatory concentrations (0.0125 mg/mL) of spike-pseudotyped lentiviruses to allow for IC formation, and then incubated these mixtures with primary human neutrophils from healthy donors. As we observed in the context of IAV, IgA–virus IC generated with IgA purified from SARS-CoV-2 convalescence serum was capable of stimulating NETosis, whereas pseudovirus–IgA mixtures from naïve serum was not (Fig. 2*B*). These results confirm that IgA–virus ICs more potently stimulate NETosis when compared to viruses alone and that ICs are required for this potentiation, since IgA from seronegative individuals did not significantly induce NETosis when mixed with pseudotyped lentivirus.

We also incubated neutrophils with antibody–HIV ICs, which contained HIV-specific IgA isolated from the serum of HIV+ individuals. Following stimulation, a significant increase in NETosis was observed in cells treated with anti-HIV IgA-containing ICs (Fig. 2*C*). Background levels of NETosis were observed when cells were treated with either IgA or viruses alone. These findings demonstrate that IgA-induced NETosis likely happens in the context of many viral infections.

NETs have also been implicated in the pathogenesis of a variety of autoimmune conditions, including RA, in which they serve as a source of autoantigen (36, 37). Patients with autoimmune diseases commonly have autoantibodies against NET elements such as histones, DNA, and neutrophil elastase. Here, neutrophils were stimulated with Ab–autoantigen ICs, composed of IgA or IgG purified from the serum of RA patients or healthy donors, and recombinant citrullinated human fibrinogen, a common autoantigen in RA (38). Induction of NETosis was observed in neutrophils stimulated with IgA–citrullinated fibrinogen ICs from RA patients but not in those stimulated with IgG-containing ICs or ICs generated with antibodies from healthy donors (Fig. 2*D*). Together, these data demonstrate that potentiation of NETosis is a common property of virus–IgA ICs as well as ICs composed of IgA–autoantigens.

Induction of NETosis by IgA ICs Is Dependent on FcαRI and Independent of TLR Signaling. We next assessed whether sIgA purified from human saliva was capable of inducing NETosis. Whereas mIgA is found predominantly in circulation, sIgA is enriched at mucosal surfaces and is generally regarded as an anti-inflammatory antibody. sIgA from saliva and serum-derived mIgA was purified from matched vaccinated donors used to generate ICs with IAV. ICs containing sIgA did not potentiate NETosis, whereas serum-derived mIgA from the same donors was capable of eliciting NETosis, as we had observed previously (Fig. 3*A*). These results are consistent with previous studies that have demonstrated that the secretory component sterically blocks binding of sIgA to FcαRI (CD89) (39).

Given the observation that sIgA–IAV ICs failed to induce NETosis, we investigated whether mIgA-mediated NETosis was dependent on engagement of FcαRI (CD89). To this end, neutrophils were incubated with a blocking monoclonal anti-CD89 antibody prior to stimulation with IgG–virus or IgA–virus ICs. Blocking with anti-CD89 abrogated induction of NETosis following stimulation with IgA ICs (Fig. 3*B*). As expected, anti-CD89 treatment had no effect on PMA-induced NETosis (*SI Appendix*, Fig. S1*B*), confirming that engagement of FcαRI is required for IgA–virus IC-mediated induction of NETosis.

TLR8 activation has been shown to shift neutrophils from phagocytosis to NETosis in the context of IgG IC-mediated NETosis via FcγRIIA signaling (32). We thus set out to determine whether TLR signaling was required for IgA-mediated NETosis induction. TLR8 senses single-stranded RNA and is an important pattern-recognition receptor during RNA virus infection (40). Since IAV particles contain RNA, we elected to use a system free from TLR7/8 ligands. To this end, polystyrene beads (roughly equal in number to IAV particles used in previous experiments) were coated with protein L and polyclonal IgA. Protein L binds to the κ-light chain of antibodies, leaving the antibody Fc region capable of interacting with FcRs on the cell surface. Following stimulation, IgA–bead ICs induced significant NETosis relative to beads alone (Fig. 3*C*). This suggests that, unlike IgG IC-mediated NETosis, IgA IC-mediated NETosis is likely independent of TLR signaling.

Neutrophils are professional phagocytes, and ADCP is one of the many Fc-mediated effector functions that contribute to their defense against pathogens (24). To directly measure whether IgA ICs induced phagocytosis, fluorescent, protein L–coated polystyrene beads were complexed with IgA or IgG prior to incubation with neutrophils. After incubation with beads, cells were washed extensively to remove any beads that had not been phagocytosed.
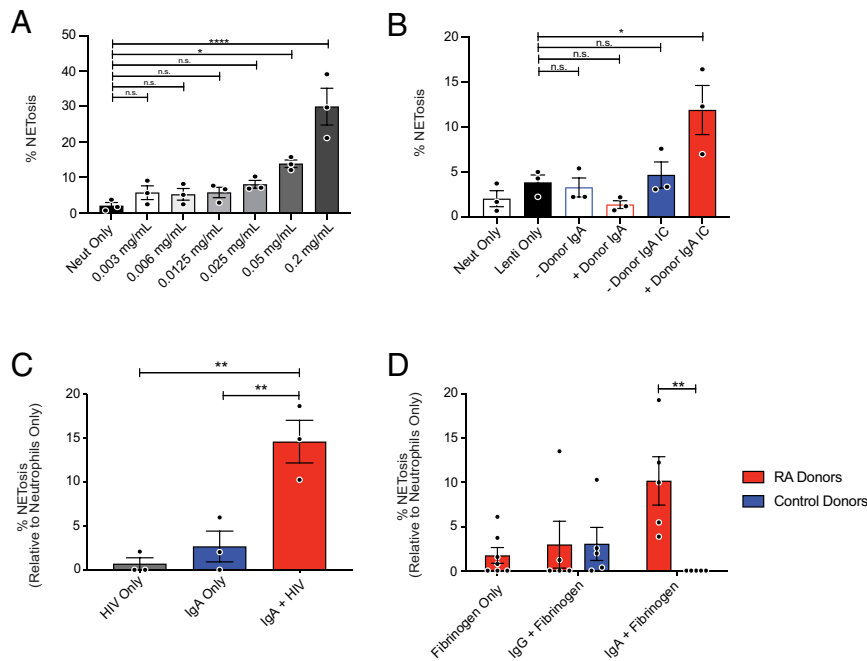
Stacey et al.
IgA potentiates NETosis in response to viral infection

PNAS | 3 of 9
https://doi.org/10.1073/pnas.2101497118

MICROBIOLOGY

Fig. 2. Potentiation of NETosis by IgA ICs is not an IAV-specific phenomenon. (*A*) Purified COVID-19 spike–pseudotyped lentivirus was titrated onto primary human neutrophils from healthy donors (*n* = 3) and incubated for 3 h prior to staining for DNA (DAPI) and neutrophil elastase. (*B*) Polyclonal IgA was isolated from serum of a convalescent COVID-19 donor and from prepandemic donor serum (COVID-19 seronegative) and incubated with spike–pseudotyped lentivirus to form ICs prior to stimulation of neutrophils isolated from healthy donors (*n* = 3) for 3 h prior to staining for DNA (DAPI) and neutrophil elastase. (*C*) ICs were formed with IgA purified from serum of HIV-positive individuals (*n* = 3) and HIV-1 X4 gp120 (HxB2)–pseudotyped lentivirus. Neutrophils were stimulated for 3 h prior to staining for DNA (DAPI) and neutrophil elastase. (*D*) Cells were stimulated with ICs containing IgA purified from the serum of healthy donors (*n* = 5) or RA patients (*n* = 5) in complex with citrullinated fibrinogen. NETosis was quantified in a blinded manner from five fields per condition. Mean and SEM of independent experiments are shown. (*A*–*C*) *P* values were determined by one-way ANOVA with Tukey post hoc test. *$P < 0.05$, **$P < 0.01$. (*D*) *P* values were determined by *t* test with multiple comparisons. *$P < 0.05$, **$P < 0.01$, ****$P < 0.0001$.

Significantly greater bead uptake was recorded for neutrophils that were exposed to the IgG-opsonized beads compared to those coated with IgA, which actually inhibited phagocytosis relative to protein L–coated control beads (Fig. 3*D*). This further demonstrates that endosomal TLR activation by viral pathogen-associated molecular patterns (PAMPs) are not required for the potentiation of NETosis by IgA–virus ICs. As further confirmation, instead of using soluble ICs, as had been done in previous experiments, ICs were immobilized on glass coverslips. Consistent with all experiments that had been performed using soluble ICs, significantly higher levels of NETosis were observed when neutrophils were incubated with immobilized IgA–virus ICs relative to immobilized IgG–virus-containing ICs (Fig. 3*E*). Combined, these data suggest that phagocytosis is not required for IgA IC-mediated stimulation of NETosis.

IgA ICs Stimulate NADPH Oxidase Complex–Dependent Suicidal NETosis. The most common and well-characterized type of NETosis is called "suicidal NETosis," which results in the death of the cell. More recently, other types of NETosis have been described, including "vital" NETosis (41). Suicidal NETosis requires ROS production and occurs between 1 and 3 h after stimulation, while vital NETosis does not require the generation of ROS and occurs between 5 and 60 min after stimulation (41). To determine whether IgA–virus IC–induced NETosis was vital or suicidal, we first performed a time-course experiment following stimulation with PMA, a well-characterized stimulant of suicidal/ROS-dependent NETosis, or IgA–IAV ICs for 0.5, 1.5, 3, or 6 h (Fig. 4*A*). A significant increase in NETosis was observed following incubation with IgA–IAV ICs for 3 h, consistent with suicidal NETosis. No further increases were observed after 6 h in either the IgG or IgA IC conditions. Unsurprisingly, PMA—a far more potent stimulant—significantly induced

NETosis beginning at 1.5 h after stimulation (Fig. 4*A*). Conversely, to inhibit the production of ROS, a small-molecule inhibitor of the NADPH oxidase (NOX) complex, diphenyleneiodonium chloride (DPI), was preincubated with neutrophils prior to stimulation with IgA–IAV ICs. DPI completely inhibited NETosis induced by IgA ICs (Fig. 4*B*). Together, these observations demonstrate that IgA–virus ICs stimulate suicidal NET release in a NOX-dependent manner.

Virus Particles Are Trapped and Inactivated by NETs. In the context of bacterial infections, NETs exert antimicrobial activity by trapping and killing bacteria with antimicrobial effector proteins associated with NETs. We thus set out to determine whether NETs were similarly capable of trapping and inactivating viruses. Neutrophils were either left unstimulated or were treated with PMA to induce suicidal NETosis (viruses containing ICs were not used to avoid the confounding issue of having viruses present during induction of NETosis). IAV was then incubated in wells of stimulated or unstimulated neutrophils, and unbound virus was washed away. Using immunofluorescence microscopy, we observed that IAV particles become trapped in NETs induced following stimulation with PMA (Fig. 4*C*). Using ImageJ software, we quantified GFP pixel density and normalized this to the number of cells (and/or NETs) per field. Consistent with the stark visual contrast observed in the images, significantly more virus was associated with PMA-stimulated neutrophils that had undergone NETosis than unstimulated neutrophils (Fig. 4*D*).

To test whether IAV was inactivated after being trapped in NETs, we used an mNeon reporter virus (42). IAV-mNeon was incubated with unstimulated neutrophils, PMA-stimulated neutrophils that had undergone NETosis, or PMA-stimulated neutrophils treated with DNase to digest NETs. DNase digestion specifically
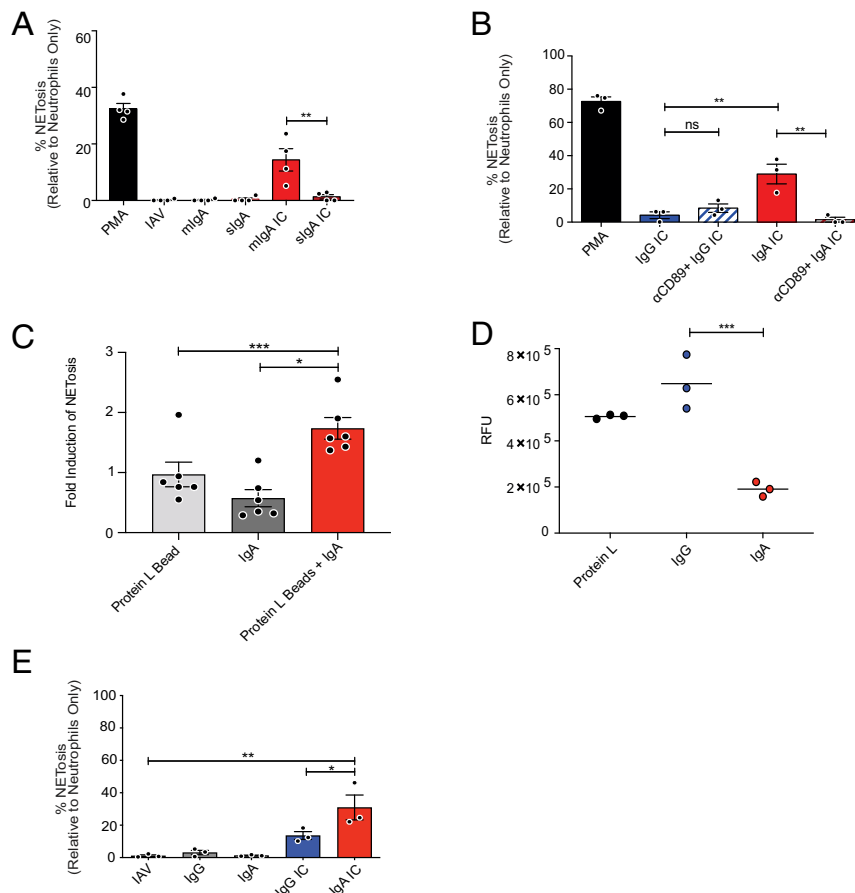
Fig. 3. IgA ICs induce NETosis via FcαRI engagement independently of TLR signaling and phagocytosis. (*A*) Primary human neutrophils were stimulated for 3 h with antibody–IAV ICs generated from matched salivary IgA and serum IgA of healthy IAV-exposed donors (*n* = 4). (*B*) Primary human neutrophils were incubated with an anti-CD89 (FcαRI) antibody prior to stimulation with IgG–IAV or IgA–IAV ICs (*n* = 3) (*C*) Primary human neutrophils were stimulated with polyclonal IgA, polystyrene beads coated with protein L, or polystyrene beads coated with protein L and IgA. For all experiments, NETosis was assessed by immunofluorescence microscopy analysis of cells costained for DNA (DAPI) and neutrophil elastase. NETosis in stimulated conditions was normalized to untreated cells (*n* = 6). (*D*) Fluorescent polystyrene beads were coated with protein L followed by either polyclonal IgG or IgA. Human neutrophils were isolated and incubated with the beads at a 500-beads-per-cell ratio. After washing, phagocytosis of beads was measured using a SpectraMax i3 plate reader (Molecular Devices) (*n* = 3). (*E*) Purified Cal/09 was immobilized on glass coverslips prior to the addition of IgG or IgA. Primary human neutrophils were added to wells for 3 h before being fixed and stained for quantification (*n* = 3). Mean and SEM of independent experiments are shown. Statistical significance was evaluated by one-way ANOVA and Tukey post hoc test. *$P < 0.05$; **$P < 0.01$, *** $P < 0.001$.

allowed us to test whether being trapped in an NET was necessary for inactivation or whether factors released by neutrophils during NETosis were alone sufficient to inactivate IAV (*SI Appendix,* Fig. S2 and Fig. 4*E*). After 3 or 6 h incubation, viral media was collected from all wells incubated on Madin Darby Canine Kidney cells (MDCKs) to quantify the remaining infectious virus. Incubation of virus with PMA-stimulated neutrophils that had undergone NETosis significantly reduced infectivity after 3 and 6 h incubation. Interestingly, digestion of NETs produced by PMA-simulated cells with DNase prior to the addition of the virus had no significant impact on infectivity, suggesting that physical contact with NETs is required for inactivation and that soluble factors released during the process of NETosis alone are not sufficient to mediated inactivation (Fig. 4*E*). Taken together, these data demonstrate that viruses can be trapped and inactivated by NETs.

Discussion

NETosis has been most extensively studied as an antipathogen immune response in the context of bacterial infections (43). However, accumulating evidence suggests that NETs have antiviral activity but can also contribute to the pathogenesis of viral disease in certain circumstances (8–11, 44, 45). While pathogens

like viruses and bacteria can trigger NETosis directly as an innate immune mechanism, there is also an important intersection of neutrophils/NETs and the adaptive immune response, since neutrophils express Fc receptors capable of recognizing both soluble ICs and antibody-bound cells. Here, we show that IgA significantly lowers the amount of virus required to trigger NETosis.

Immobilized IgG ICs have been reported to stimulate NETosis via FcγRIIA. Soluble ICs were primarily phagocytosed but could be shifted to stimulate NETosis upon TLR7/8 activation, which resulted in furin-mediated cleavage and shedding of the FcγRIIA N terminus—inhibiting further phagocytosis (32). We observed that IgA ICs did not simulate phagocytosis but rather preferentially induced NETosis even in the absence of TLR activation. While IgG ICs could stimulate NETosis, the induction of NETosis was notably more pronounced upon stimulation of neutrophils with IgA ICs.

In the context of IAV, bnAbs that bind to the conserved HA stalk domain have become a major focus for the development of "universal" influenza virus vaccines and monoclonal antibody prophylactics/therapeutics. Although bnAbs are relatively weak neutralizers of IAV, they confer protection in vivo via potent induction of Fc-dependent effector functions (17–19, 22, 24, 26, 27).
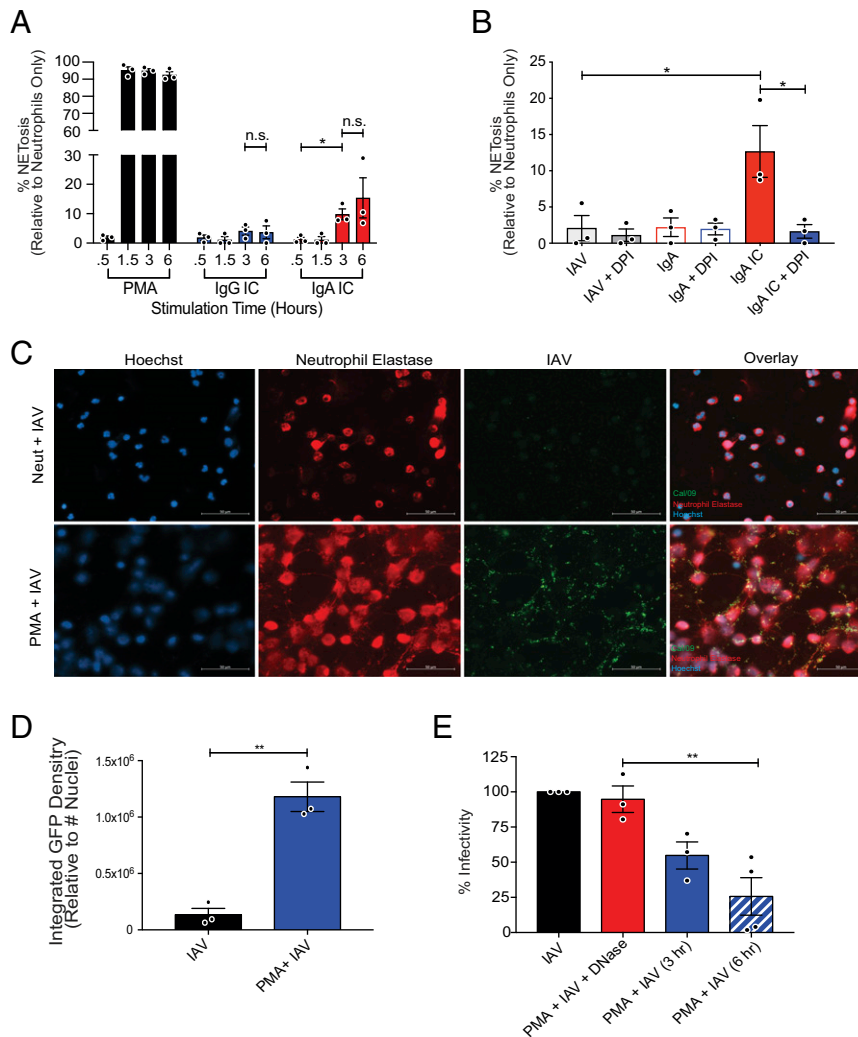
Stacey et al.
IgA potentiates NETosis in response to viral infection

PNAS | 5 of 9
https://doi.org/10.1073/pnas.2101497118

Fig. 4. Influenza virus particles are trapped and inactivated by NETs released via suicidal NETosis. (*A*) Primary human neutrophils were stimulated with PMA, IgG–IAV, or IgA–IAV ICs for 0.5, 1.5, 3, or 6 h prior to fixation and staining for DNA (DAPI) and neutrophil elastase to quantify NETosis. (*B*) Primary human neutrophils were incubated with DPI, a NOX inhibitor, prior to 3 h of simulation with IgA–IAV ICs (*n* = 3). (*C*) Neutrophils were stimulated with PMA for 90 min before the addition 10^5 PFU per well of IAV. The virus was incubated with the NETs for 3 h and then fixed and stained with anti-hemagglutinin antibodies (6F12), DNA (Hoechst), and neutrophil elastase. Immunofluorescence microscopy was used to measure the colocalization of viral particles (green) with NETs composed of DNA (blue) coated with neutrophil elastase (red) (*n* = 3) (*D*) Quantification of the raw integrated GFP density was measured using ImageJ and normalized to the number of cells per field. (*E*) Neutrophils were stimulated with PMA prior to the addition of an IAV expressing an mNeon reporter. The virus was incubated on intact NETs or NETs that had been digested with DNase (*n* = 3). The contents of wells were collected, and MDCK cells were infected for 8 h to measure residual infectivity. Mean and ± SEM are shown. Statistical significance was evaluated using one-way ANOVA with Tukey post hoc test. *$P <$ 0.05; **$P <$ 0.01.

The ability of bnAbs to elicit potent effector functions (relative to conventional neutralizing antibodies that bind to the HA head domain) relies on a unique reciprocal contact model, whereby Fc receptors of immune-effector cells bind to the Fc domain of bnAbs bound to HA on target cells, while HA expressed on target cells, in turn, binds to sialic acid residues of the effector cell (26, 27). However, almost everything that is known about the function of bnAbs has been studied in the context of IgG. Of the other immunoglobulin isotypes, IgA plays a particularly important role in protection against mucosal viruses. Indeed, local IgA responses correlate with protection offered by live-attenuated influenza virus vaccines (46–48). A recent Phase-I trial of a chimeric HA universal vaccine candidate reported potent induction of IgA bnAbs after vaccination, further highlighting the urgent need to understand how antibodies of this isotype contribute to protection (20, 49). Here, we show that, consistent with prior studies, bnAbs are

primarily responsible for the induction of FcαRI-dependent NETosis, likely because these antibodies also promote the reciprocal binding events between IgA–FcαRI and HA–sialic acid (50).

Importantly, the ability of IgA ICs to potentiate NETosis was widespread across several different viruses including IAV, lentiviruses pseudotyped with the SARS-CoV-2 S protein, and HIV. Indeed, this phenomenon could also be recapitulated with IgA-coated beads and extended beyond the context of infectious diseases to ICs composed of IgA from RA patients in complex with citrullinated fibrinogen—a common RA autoantigen. Our findings support previous work from the van Egmond laboratory demonstrating that IgA ICs isolated from synovial fluid of RA patients also induce NETosis (36). Previous work by our group has shown that, upon exposure to IgG–IAV ICs, neutrophils undergo ADCP and potently induce ROS. Inhibition of phagocytosis with cytochalasin D almost completely abolished ROS

induction by IgG–IAV ICs. In contrast, IgA–IAV ICs were able to stimulate ROS even when phagocytosis was inhibited (24). Those observations are in line with the data presented herein showing that IgA–ICs induced neutrophils to undergo ROS-dependent suicidal NETosis in a phagocytosis-independent manner.

In serum, IgA is present at concentration of ~82 to 624 mg/dL, whereas IgG is found at ~694 to 1,803 mg/dL (51). The antibody distribution in tissues has been estimated to be 4 to 16% of the plasma concentration (52). Thus, the concentrations of antibodies that we have used in this study (50 to 100 μg/mL or 5 to 10 mg/dL) were chosen to reflect these physiologically relevant conditions. In serum, IgA1 is the dominant subclass, existing at a ratio of roughly 9:1 when compared to IgA2. We therefore used monoclonal IgA1 antibodies in our studies However, IgA2 antibodies were recently shown to induce more potent inflammatory signaling through FcαRI than IgA1 antibodies, perhaps due to differences in their glycosylation profiles (53). Thus, in contexts wherein IgA2 is enriched, such as in mucosal tissues or in the context of certain autoimmune diseases, the potentiation of NETosis may be even more potent.

In the context of HIV, mixed IgG/IgA–HIV ICs generated using the gp41-specific bnAb 2F5 cooperatively triggered ADCC of HIV-infected cells by monocytes but did not act cooperatively to induce ADCP (33, 54). Likewise, we observed no cooperativity in the induction of NETosis when IgA and IgG were combined at a 1:1 ratio or at physiological ratios. These results suggest that signaling downstream of FcγRs and FcαRI leads to distinct effector outcomes in monocytes and neutrophils.

While ICs composed of serum-derived IgA and monomeric monoclonal IgA could both potentiate NETosis, sIgA purified from saliva could not. This is consistent with prior studies that have demonstrated that the secretory component sterically interferes with binding to FcαRI and suggests that IgA-stimulated NETosis is unlikely to occur in the airways in which sIgA is enriched, but instead would be expected to take place primarily in tissues and vasculature (55).

The data presented here demonstrate that NETs can both trap and inactivate viruses. This suggests that they may have a protective antiviral function. NETs are decorated with antimicrobial proteins including myeloperoxidase, and cationic peptides like α-defensin and cathelicidins that are known to inactivate viral particles (56, 57). We speculate that, in individuals who lack virus-specific IgA, the high concentrations of virus needed to stimulate NETosis might exacerbate inflammation and potentiate disease as has been observed for those with COVID-19 (14–16, 35). However, for individuals with preexisting immunity—such as that conferred by vaccines—low levels of IgA-induced NETosis might help to trap and inactivate viruses early in infection, thereby limiting virus spread and progression to severe disease.

In summary, we report an antiviral effector function mediated by virus–IgA ICs. The mechanism through which virus–IgA ICs stimulate NETosis is distinct from—and considerably more potent than—virus alone. Since mice do not express an FcαR, it will be important to develop alternative models for in vivo studies to determine when IgA–virus IC-mediated NETosis may be protective and when it may exacerbate disease.

Materials and Methods

Human Serum and Blood Samples. Human blood samples used to isolate serum antibodies were obtained with permission from consenting male and female IAV-vaccinated donors, SARS-CoV-2 infected donors, HIV-positive individuals, and RA patients. Human blood for neutrophil isolations was collected with permission from consenting healthy male and female donors. All protocols involving human samples were approved by the Hamilton Integrated Research Ethics Board and the Western Research Ethics Board. Blood was collected into ethylenediaminetetraacetic acid (EDTA) coated tubes (BD Vacutainer).

Neutrophil Isolation. Neutrophils were isolated from the peripheral blood of healthy male and female donors by density gradient centrifugation as described previously (24). Briefly, 3 mL room-temperature (RT) Histopaque 1119 (Sigma-Aldrich) was added to a 15-mL falcon tube followed by gentle addition of 3 mL Histopaque 1077 (Sigma- Aldrich). A total of 6 mL blood was layered on top, and samples were centrifuged at $930 \times g$ for 30 min at RT with no deceleration in an Allegra X-12R centrifuge (Beckman Coulter). The neutrophil layer was collected between the Histopaque layers and diluted in 4 °C polymorphonuclear cell (PMN) buffer (0.5% bovine serum albumin [BSA], 0.3 mM EDTA in Hank's balanced salt solution [Sigma-Aldrich]) to a total volume of 50 mL. PMNs were then centrifuged at $450 \times g$ for 5 min at RT. The supernatant was discarded, and the cell pellet was resuspended by flicking the tube. To lyse red blood cells, 3 mL ammonium-chloride-potassium lysis buffer (8.3 g/L NH_4Cl, 1 g/L $KHCO_3$, and 0.05 mM EDTA, in sterile distilled H_2O) was added to the PMNs and incubated for 3 min with agitation every 30 s. The PMNs were diluted in 30 mL PMN buffer and centrifuged at $450 \times g$ for 5 min at RT followed by one additional wash.

Antibody Purification. Heat-inactivated human serum was diluted 1:10 in phosphate-buffered saline (PBS) and applied to a gravity polypropylene flow column (Qiagen) containing 1 mL Protein G-Sepharose resin (Invitrogen) to purify IgG. Flow through sera was then applied to a gravity flow column containing 1 mL Peptide M-Sepharose resin (InvivoGen) to purify IgA. Columns were washed with two column volumes of PBS. IgG and IgA were eluted with 0.1 M glycine-HCl buffer (pH 2.7) into 2 M Tris·HCl neutralizing buffer (pH 10). Antibodies were concentrated and resuspended in PBS using 30 kDa cutoff Macrosep Advanced Centrifugal Devices (Pall Corporation). To purify monoclonal antibodies, clarified cell-culture supernatants were applied directly to Protein G-Sepharose columns prior to washing and elution.

Monoclonal Antibodies. The variable light and heavy chain sequences of KB2 and 29E3 antibodies (30, 58) were cloned into pFuse vectors (pFUSE-CHIg-hG1, pFUSEss-CHIg hA1, and pFUSE2ss-CLIg-hK, Invivogen). KB2 binds to the stalk domain of H1 viruses, while the 29E3 antibody is specific to the head domain of Cal/09. HEK293T cells were cotransfected with pFUSE plasmids according to the manufacturer's recommendations, and antibodies were subsequently purified from supernatants using Protein G-Sepharose columns as described (see *Antibody Purification*).

Cells and Viruses. MDCK cells were grown in Dulbecco modified Eagle medium (DMEM) containing 10% fetal bovine serum (FBS) (Gibco), 2 mM L-glutamine, and 100 U/mL penicillin-streptomycin (Thermo Fisher Scientific). At 100% confluency, MDCK cells were infected for 1 h with Cal/09 H1N1 (kind gift of Peter Palese, Icahn School of Medicine at Mount Sinai, New York, NY) in 1× minimum essential medium (MEM, Sigma-Aldrich) supplemented with 2 mM L-glutamine, 0.24% sodium bicarbonate, 20 mM Hepes [4-(2-hydroxyethyl)-1-piperazineethanesulfonic acid], MEM amino acids solution (Sigma-Aldrich), MEM vitamins solution (Sigma-Aldrich), 100 U/mL penicillin-streptomycin (Thermo Fisher Scientific), and 0.42% BSA (Sigma-Aldrich). Cells were then washed with PBS, and media were replaced. Cells were left for 72 h, and supernatant was collected. A/Puerto Rico/8/1934/H1N1-mNeon (PR8-mNeon), which was a kind gift from the laboratory of Nicholas Heaton (Duke University, Durham, NC) (42), was propagated in 10-d-old embryonated chicken eggs as per standard protocols (59).

Influenza Virus Purification. Clarified supernatants from IAV-infected MDCK cells were layered on top of 8 mL 20% sucrose (Bioshop) in NTE buffer (0.5 M NaCl, 10 mM Tris·HCl, 1 mM EDTA, pH 7.5) inside Ultra-Clear Ultracentrifuge tubes (Beckman Coulter). Samples were spun at $76,650 \times g$ for 2 h at 4 °C inside a SW 32i rotor using an Optima L-90K Ultracentrifuge (Beckman Coulter). Purified viruses were quantified using a bicinchoninic acid assay (BCA) Protein Assay Kit (Pierce Biotechnology) according to the manufacturer's instructions and by hemagglutination assay.

Pseudotyped Lentivirus Production. HIV-1 X4 gp120-pseudotyped lentiviruses were prepared described previously (60). Briefly, HEK293T cells were cultured in DMEM supplemented with 10% FBS, L-glutamine, and 100 U/mL penicillin-streptomycin and maintained in 5% CO_2 at 37 °C. Briefly, 5×10^5 cells were seeded onto 6-well plates 1 d prior to transfection. Cells were cotransfected on the next day at 70 to 80% confluency with pLenti-CMV-GFP-Puro (1.5 μg) along with pEnv$_{HxB}$ (0.5 μg) and psPAX2 (1 μg) plasmids. The medium was changed 24 h posttransfection. The supernatant was then harvested, filtered with 0.22-μm filters (Millipore), and titered as described previously (60). The virus was stored at −80 °C until use.

Stacey et al.
IgA potentiates NETosis in response to viral infection

PNAS | 7 of 9
https://doi.org/10.1073/pnas.2101497118

SARS-CoV-2 S protein–pseudotyped lentiviruses were produced as described by Crawford et al. (61), and the following reagents were obtained through the Biodefense and Emerging Infections Research Resources Repository (BEI Resources), National Institute of Allergy and Infectious Diseases (NIAID), NIH: SARS-Related Coronavirus 2, Wuhan-Hu-1 Spike-Pseudotyped Lentiviral Kit, NR-52948. In brief, HEK293T cells seeded in 15-cm dishes at 1.1×10^7 cells/mL in 15 mL standard DMEM. A total of 16 to 24 h postseeding, cells were cotransfected with HDM-nCoV-Spike-IDTopt-ALAYT, pHAGE-CMV-Luc2-IRES-ZsGreen-W (BEI catalog number NR-52516), HDM-Hgpm2 (BEI catalog number NR-52517) HDM-tat1b (BEI catalog number NR-52518), and pRC-CMV-Rev1b (BEI catalog NR-52519). A total of 18 to 24 h posttransfection, the media were replaced with full DMEM. A total of 60 h posttransfection, the supernatant was collected and filtered with a 0.45-μm filter and stored at −80° C. For purification, 40 mL supernatant was concentrated by spinning at 19,400 rpm for 2 h in an SW 32 Ti rotor using a Beckman Coulter Optima L-90K ultracentrifuge. The resulting pellet was resuspended in 400 μl Hank's Balanced Salt Solution (HBSS) followed by 15 min of continuous vortex at RT. The protein concentration was confirmed by BCA.

Coating Polystyrene Microspheres with Protein L and a Polyclonal Antibody. Fluorescent carboxylate microspheres of 0.5 μm (Polysciences) were coated with Protein L (Thermo Fisher Scientific) followed by polyclonal IgA or IgG. The polystyrene microspheres were first washed with 1× PBS and centrifuged at $13,523 \times g$. The PBS wash was repeated, and then the microspheres were incubated at RT with 750 μg Protein L for 4 h with gentle mixing. Following another PBS wash, 300 μg polyclonal IgA was added to the microspheres and left to incubate at RT with gentle mixing overnight. Following this incubation, the microspheres were centrifuged at $13,523 \times g$ for 10 min, and the resulting pellet was resuspended in 1 mL PBS for 30 min with gentle mixing at RT. Following the final incubation, the microspheres were centrifuged at $13,523 \times g$ for 5 min and resuspended in 500 μL PBS.

Neutrophil Stimulation with Soluble ICs. Glass coverslips of 15 mm were placed inside wells of a sterile 24-well plate, and 4.0×10^5 PMNs were added to each well and allowed to settle for 1 h. For IAV–polyclonal Ab stimulations, mixtures of 25 μg Cal/09 (2^{10} hemaglutinin units (HAU)) and 50 μg/mL polyclonal IgG or IgA antibodies were incubated for 30 min at RT before addition to PMNs. ICs containing monoclonal HA stalk (KB2) or head-binding (29E3) antibodies were generated at a 2:1 ratio of antibody to virus (100 μg/mL and 50 μg/mL, respectively) and allowed to incubate for 30 min at RT prior to stimulation of PMNs. To test the ability of ICs generated with sIgA to stimulate NETosis, matched sIgA and serum IgA were purified from the saliva of four healthy donors using peptide M columns. ICs containing 100 μg per well of serum-derived monomeric IgA or sIgA and 50 μg per well of Cal/09 were allowed to form by incubation at RT 30 min. HIV-specific ICs were generated by purifying IgA from the serum of three HIV-1–positive donors. ICs were formed by incubating 100 μg/mL polyclonal IgA and 50 μg/mL HIV-1 gp120-pseudotyped lentiviruses for 30 min at RT. SARS-CoV-2 ICs were generated using antibodies purified from the convalescent sera of an individual who had been infected with SARS-CoV-2. ICs were formed by incubating 100 μg/mL polyclonal IgA and 12.5 μg/mL pseudotyped spike lentiviruses for 30 min at RT. For RA samples, ICs were formed by incubating 50 μg per well of citrullinated human fibrinogen (Cayman Chemicals) with 100 μg per well of polyclonal IgA or IgG for 30 min at RT. Stimulation of IgA-coated beads was performed by incubating neutrophils with 5.0×10^8 beads. Antibodies/viruses/beads/ICs were then incubated with PMNs for 3 h at 37 °C before being fixed with 3.7% paraformaldehyde (PFA) (Pierce Protein Biology) prior to staining and imaging.

Immobilized IC Assay. Purified viruses were plated on 15-mm sterile coverslips in a 24-well plate at 2 μg/mL and incubated at 37 °C for 18 h. Wells were washed twice with PBS, and 250 μg of either polyclonal IgA or IgG was added for 30 min at 37 °C. Wells were washed twice with PBS prior to the addition of 4.0×10^5 PMNs per well. PMNs were incubated for 3 h at 37 °C, fixed, and stained (see *Fluorescence Microscopy and Quantification of NETosis*).

FcαRI Blockade. Glass coverslips of 15 mm were placed inside wells of a sterile 12-well plate, and 4.0×10^5 PMNs were added to each well in a total volume of 500 μL and allowed to settle for 1 h. To block Fc-αRI, 20 μg/mL mouse anti-human CD89 antibody (AbD Serotec) was added to neutrophils for 20 min at 4 °C. PMNs were then stimulated with various conditions for 3 h at 37 °C before being fixed with 3.7% PFA and stored at 4 °C until staining.

Fluorescence Microscopy and Quantification of NETosis. Cells were fixed with 3.7% PFA (Pierce Protein Biology) at 4 °C, washed in PBS three times, and then permeabilized using 0.5% Triton X-100 (Thermo Fisher Scientific) in phosphate-

buffered saline, 0.1% Tween (PBS-T). Fixed and permeabilized cells were then blocked for 30 min at RT in blocking buffer (10% FBS in PBS-T). Cells were incubated with primary rabbit anti-neutrophil elastase antibody (Abcam) at a 1:100 dilution for 1 h at RT. Coverslips were washed with PBS three times and then incubated with Alexa Fluor 488-conjugated donkey anti-rabbit antibody (Molecular Probes) diluted as per the manufacturer's recommendation (two drops per milliliter) for 1 h at RT, protected from light. Coverslips were then washed with PBS three times. A total of 1 μg/mL Hoechst 33342, trihydrochloride, trihydrate (Life Technologies) was incubated for 5 min at RT, protected from light. Cells were washed with PBS three times, and coverslips were mounted onto glass slides in EverBrite Mounting Medium (Biotium). Cells were imaged using an EVOS FL microscope (Life Technologies). Five random fields per condition were captured at 20× magnification. NETosis was quantified by counting cells that had decondensed chromatin colocalized with neutrophil elastase. Percent NETosis was expressed as the number of cells that had undergone NETosis/the number of total cells.

Influenza Viral-Particle Trapping and Inactivation in NETs. Sterilized glass coverslips were placed in a 24 well plate, and neutrophils at 4.0×10^5 cells per well were allowed to settle for 1 h prior to stimulation. Neutrophils were stimulated with PMA for 3 h at 37 °C, 5% CO_2. Cal/09 at 10^5 PFU/mL was then allowed to settle on the preformed NETs for 3 h at 37 °C; following this, incubation cells were fixed with 3.7% PFA. Staining was performed as previously described (see *Fluorescence Microscopy and Quantification of NETosis*). Primary antibodies used included the following: primary rabbit anti-neutrophil elastase antibodies (Abcam, 1:100 dilution) and 6F12 generated from in-house hybridomas at 1 μg/mL. Secondary antibodies included the following: Alexa Fluor 488 conjugated donkey anti-mouse antibodies (Molecular Probes, 1:4,000) and Alexa Flour 594 donkey anti-rabbit (Molecular Probes, 1:4,000). Coverslips were incubated with 1 μg/mL Hoechst 33342, trihydrochloride, trihydrate (Life Technologies) to probe for DNA. Cells were visualized and imaged using GFP (Ex 470 nm/Em 525 nm) and DAPI (Ex 360 nm/Em 447 nm), with Texas Red (Ex 585/Em 624) color cubes in the EVOS FL microscope (Life Technologies). To evaluate inactivation, 10^5 PFU/mL of PR8-mNeon was incubated with PMA-stimulated neutrophils for 3 to 6 h. A total of 25 units per milliliter of DNaseI (Thermo Fisher Scientific) were added to PMA-stimulated neutrophils and were allowed to incubate for 90 min to digest NETs. Samples were collected and stored at −80° C until further use. Prior to virus quantification, MDCK cells were seeded in 24-well plates and used when 90% confluent. The sample was diluted 1:10 in 1× MEM (Sigma-Aldrich), supplemented with 2 mM L-glutamine, 0.24% sodium bicarbonate, 20 mM Hepes, MEM amino acids solution (Sigma-Aldrich), MEM vitamins solution (Sigma-Aldrich), 100 U/mL penicillin-streptomycin (Thermo Fisher Scientific), and 0.42% BSA (Sigma-Aldrich), before being added to cells. After 1 h, this was replaced with DMEM containing 10% FBS (Gibco), 2 mM L-glutamine, and 100 U/mL penicillin-streptomycin. The number of fluorescent cells was assessed 12 h postinfection. Cells were fixed with PFA and incubated with 1 μg/mL Hoechst 33342, trihydrochloride, trihydrate (Life Technologies). Five fields per condition were taken on the EVOS FL microscope, and percent infectivity was determined as the number of infected cells/the total number of cells.

Phagocytosis Assay of Polyclonal Antibody–Coated Microspheres. This protocol was performed as previously described (24). Briefly, fluorescent carboxylate microspheres of 0.5 μm (Polysciences) were coated with protein L and polyclonal IgA or IgG and were incubated with neutrophils at a 500:1 ratio at 37 °C for 15 min with gentle mixing. This was followed by centrifugation at $930 \times g$ for 10 min. Cells were washed twice with PBS before being plated in a 96-well plate. Fluorescence was measured with the SpectraMax i3 plate reader at 526 nm (Molecular Devices).

NOX Assay. Neutrophils were purified as described above (see *Neutrophil Isolation*) and allowed to settle on glass coverslips for 1 h at 37 °C. While settling, neutrophils were incubated with 20 μm DPI (Sigma-Aldrich), a neutrophil NADPH oxidase inhibitor. Neutrophils were then stimulated with IgA–IAV ICs or PMA (0.1 mg/mL, Sigma-Aldrich) as a positive control, and DPI was maintained in the media. Cells were then fixed with 3.7% PFA and stored at 4 °C until staining and imaging.

Statistics. Graphs and statistical analyses were generated using Graphpad Prism version 9 (GraphPad Software). $P < 0.05$ was considered to be significant across all experiments.

Data Availability. All study data are included in the article and/or *SI Appendix*.

1. J. E. Bakema, M. van Egmond, The human immunoglobulin A Fc receptor FcαRI: A multifaceted regulator of mucosal immunity. *Mucosal Immunol.* **4**, 612–624 (2011).
2. E. Kolaczkowska, P. Kubes, Neutrophil recruitment and function in health and inflammation. *Nat. Rev. Immunol.* **13**, 159–175 (2013).
3. R. C. Monteiro, J. G. J. Van De Winkel, IgA Fc receptors. *Annu. Rev. Immunol.* **21**, 177–204 (2003).
4. V. Papayannopoulos, Neutrophil extracellular traps in immunity and disease. *Nat. Rev. Immunol.* **18**, 134–147 (2018).
5. J. V. Camp, C. B. Jonsson, A role for neutrophils in viral respiratory disease. *Front. Immunol.* **8**, 550 (2017).
6. V. Brinkmann *et al.*, Neutrophil extracellular traps kill bacteria. *Science* **303**, 1532–1535 (2004).
7. C. H. Hiroki *et al.*, Neutrophil extracellular traps effectively control acute Chikungunya virus infection. *Front. Immunol.* **10**, 3108 (2020).
8. C. N. Jenne *et al.*, Neutrophils recruited to sites of infection protect from virus challenge by releasing neutrophil extracellular traps. *Cell Host Microbe* **13**, 169–180 (2013).
9. T. Saitoh *et al.*, Neutrophil extracellular traps mediate a host defense response to human immunodeficiency virus-1. *Cell Host Microbe* **12**, 109–116 (2012).
10. P. S. Sung, T. F. Huang, S. L. Hsieh, Extracellular vesicles from CLEC2-activated platelets enhance dengue virus-induced lethality via CLEC5A/TLR2. *Nat. Commun.* **10**, 2402 (2019).
11. B. Cortjens *et al.*, Neutrophil extracellular traps cause airway obstruction during respiratory syncytial virus disease. *J. Pathol.* **238**, 401–411 (2016).
12. M. Toussaint *et al.*, Host DNA released by NETosis promotes rhinovirus-induced type-2 allergic asthma exacerbation. *Nat. Med.* **23**, 681–691 (2017).
13. T. Narasaraju *et al.*, Excessive neutrophils and neutrophil extracellular traps contribute to acute lung injury of influenza pneumonitis. *Am. J. Pathol.* **179**, 199–210 (2011).
14. C. Radermecker *et al.*, Neutrophil extracellular traps infiltrate the lung airway, interstitial, and vascular compartments in severe COVID-19. *J. Exp. Med.* **217**, e20201012 (2020).
15. E. A. Middleton *et al.*, Neutrophil extracellular traps contribute to immunothrombosis in COVID-19 acute respiratory distress syndrome. *Blood* **136**, 1169–1179 (2020).
16. B. J. Barnes *et al.*, Targeting potential drivers of COVID-19: Neutrophil extracellular traps. *J. Exp. Med.* **217**, e20200652 (2020).
17. D. J. DiLillo, P. Palese, P. C. Wilson, J. V. Ravetch, Broadly neutralizing anti-influenza antibodies require Fc receptor engagement for in vivo protection. *J. Clin. Invest.* **126**, 605–610 (2016).
18. D. J. DiLillo, G. S. Tan, P. Palese, J. V. Ravetch, Broadly neutralizing hemagglutinin stalk-specific antibodies require FcγR interactions for protection against influenza virus in vivo. *Nat. Med.* **20**, 143–151 (2014).
19. W. He *et al.*, Alveolar macrophages are critical for broadly-reactive antibody-mediated protection against influenza A virus in mice. *Nat. Commun.* **8**, 846 (2017).
20. D. I. Bernstein *et al.*, Immunogenicity of chimeric haemagglutinin-based, universal influenza virus vaccine candidates: Interim results of a randomised, placebo-controlled, phase 1 clinical trial. *Lancet Infect. Dis.* **20**, 80–91 (2019).
21. D. N. Forthal, A. Finzi, Antibody-dependent cellular cytotoxicity in HIV infection. *AIDS* **32**, 2439–2451 (2018).
22. W. He *et al.*, Broadly-neutralizing anti-influenza virus antibodies: Enhancement of neutralizing potency in polyclonal mixtures and IgA backbones. *J. Virol.* **89**, 3610–3618 (2015).
23. M. D. Tate *et al.*, Neutrophils ameliorate lung injury and the development of severe disease during influenza infection. *J. Immunol.* **183**, 7441–7450 (2009).
24. C. E. Mullarkey *et al.*, Broadly neutralizing hemagglutinin stalk-specific antibodies induce potent phagocytosis of immune complexes by neutrophils in an Fc-dependent manner. *mBio* **7**, e01624-16 (2016).
25. T. A. Fuchs *et al.*, Novel cell death program leads to neutrophil extracellular traps. *J. Cell Biol.* **176**, 231–241 (2007).
26. W. He *et al.*, Epitope specificity plays a critical role in regulating antibody-dependent cell-mediated cytotoxicity against influenza A virus. *Proc. Natl. Acad. Sci. U.S.A.* **113**, 11931–11936 (2016).
27. P. E. Leon *et al.*, Optimal activation of Fc-mediated effector functions by influenza virus hemagglutinin antibodies requires two points of contact. *Proc. Natl. Acad. Sci. U.S.A.* **113**, E5944–E5951 (2016).
28. G. S. Tan *et al.*, A pan-H1 anti-hemagglutinin monoclonal antibody with potent broad-spectrum efficacy in vivo. *J. Virol.* **86**, 6179–6188 (2012).
29. G. S. Tan *et al.*, Characterization of a broadly neutralizing monoclonal antibody that targets the fusion domain of group 2 influenza A virus hemagglutinin. *J. Virol.* **88**, 13580–13592 (2014).
30. N. S. Heaton *et al.*, In vivo bioluminescent imaging of influenza a virus infection and characterization of novel cross-protective monoclonal antibodies. *J. Virol.* **87**, 8272–8281 (2013).
31. R. Hai *et al.*, Influenza viruses expressing chimeric hemagglutinins: Globular head and stalk domains derived from different subtypes. *J. Virol.* **86**, 5774–5781 (2012).
32. C. Lood, S. Arve, J. Ledbetter, K. B. Elkon, TLR7/8 activation in neutrophils impairs immune complex phagocytosis through shedding of FcgRIIA. *J. Exp. Med.* **214**, 2103–2119 (2017).
33. M. Duchemin, D. Tudor, A. Cottignies-Calamarte, M. Bomsel, Antibody-dependent cellular phagocytosis of HIV-1-Infected cells is efficiently triggered by IgA targeting HIV-1 envelope subunit gp41. *Front. Immunol.* **11**, 1141 (2020).
34. F. P. Veras *et al.*, SARS-CoV-2-triggered neutrophil extracellular traps mediate COVID-19 pathology. *J. Exp. Med.* **217**, e20201129 (2020).
35. Y. Zuo *et al.*, Neutrophil extracellular traps in COVID-19. *JCI Insight* **5**, e138999 (2020).
36. E. Aleyd, M. Al, C. W. Tuk, C. J. van der Laken, M. van Egmond, IgA complexes in plasma and synovial fluid of patients with rheumatoid arthritis induce neutrophil extracellular traps via FcαRI. *J. Immunol.* **197**, 4552–4559 (2016).
37. H. L. Wright, R. J. Moots, S. W. Edwards, The multifactorial role of neutrophils in rheumatoid arthritis. *Nat. Rev. Rheumatol.* **10**, 593–601 (2014).
38. J. A. Hill, J. Al-Bishri, D. D. Gladman, E. Cairns, D. A. Bell, Serum autoantibodies that bind citrullinated fibrinogen are frequently found in patients with rheumatoid arthritis. *J. Rheumatol.* **33**, 2115–2119 (2006).
39. A. B. Herr, E. R. Ballister, P. J. Bjorkman, Insights into IgA-mediated immune responses from the crystal structures of human FcalphaRI and its complex with IgA1-Fc. *Nature* **423**, 614–620 (2003).
40. F. Heil *et al.*, Species-specific recognition of single-stranded RNA via toll-like receptor 7 and 8. *Science* **303**, 1526–1529 (2004).
41. B. G. Yipp, P. Kubes, NETosis: How vital is it? *Blood* **122**, 2784–2794 (2013).
42. A. T. Harding, B. E. Heaton, R. E. Dumm, N. S. Heaton, Rationally designed influenza virus vaccines that are antigenically stable during growth in eggs. *mBio* **8**, e00669-17 (2017).
43. V. Papayannopoulos, A. Zychlinsky, NETs: A new strategy for using old weapons. *Trends Immunol.* **30**, 513–521 (2009).
44. L. Zhu *et al.*, High level of neutrophil extracellular traps correlates with poor prognosis of severe influenza A infection. *J. Infect. Dis.* **217**, 428–437 (2018).
45. C. N. Jenne, P. Kubes, Virus-induced NETs–critical component of host defense or pathogenic mediator? *PLoS Pathog.* **11**, e1004546 (2015).
46. C. S. Ambrose, X. Wu, T. Jones, R. M. Mallory, The role of nasal IgA in children vaccinated with live attenuated influenza vaccine. *Vaccine* **30**, 6794–6801 (2012).
47. D. F. Hoft *et al.*, Comparisons of the humoral and cellular immune responses induced by live attenuated influenza vaccine and inactivated influenza vaccine in adults. *Clin. Vaccine Immunol.* **24**, e00414-16 (2017).
48. J. C. Ang *et al.*, Comparative immunogenicity of the 2014-2015 Northern hemisphere trivalent IIV and LAIV against influenza A viruses in children. *Vaccines (Basel)* **7**, 87 (2019).
49. R. Nachbagauer *et al.*, A chimeric hemagglutinin-based universal influenza virus vaccine approach induces broad and long-lasting immunity in a randomized, placebo-controlled phase I trial. *Nat. Med.* **27**, 106–114 (2020).
50. A. W. Freyn *et al.*, Influenza hemagglutinin-specific IgA Fc-effector functionality is restricted to stalk epitopes. *Proc. Natl. Acad. Sci. U.S.A.* **118**, e2018102118 (2021).
51. A. Gonzalez-Quintela *et al.*, Serum levels of immunoglobulins (IgG, IgA, IgM) in a general adult population and their relationship with alcohol consumption, smoking and common metabolic abnormalities. *Clin. Exp. Immunol.* **151**, 42–50 (2008).
52. D. K. Shah, A. M. Betts, Antibody biodistribution coefficients: Inferring tissue concentrations of monoclonal antibodies based on the plasma concentrations in several preclinical species and human. *mAbs* **5**, 297–305 (2013).
53. U. Steffen *et al.*, IgA subclasses have different effector functions associated with distinct glycosylation profiles. *Nat. Commun.* **11**, 120 (2020).
54. M. Duchemin, M. Khamassi, L. Xu, D. Tudor, M. Bomsel, IgA targeting human immunodeficiency virus-1 envelope gp41 triggers antibody-dependent cellular cytotoxicity cross-clade and cooperates with gp41-specific IgG to increase cell lysis. *Front. Immunol.* **9**, 244 (2018).
55. E. Aleyd, M. H. Heineke, M. van Egmond, The era of the immunoglobulin A Fc receptor FcαRI; its function and potential as target in disease. *Immunol. Rev.* **268**, 123–138 (2015).
56. G. Schönrich, M. J. Raftery, Neutrophil extracellular traps go viral. *Front. Immunol.* **7**, 366 (2016).
57. E. Gwyer Findlay, S. M. Currie, D. J. Davidson, Cationic host defence peptides: Potential as antiviral therapeutics. *BioDrugs* **27**, 479–493 (2013).
58. B. Manicassamy *et al.*, Protection of mice against lethal challenge with 2009 H1N1 influenza A virus by 1918-like and classical swine H1N1 based vaccines. *PLoS Pathog.* **6**, e1000745 (2010).
59. WHO, Manual for the laboratory diagnosis and virological surveillance of influenza. (2011). https://apps.who.int/iris/handle/10665/44518. Accessed 4 March 2015.
60. M. A. Zahoor, S. Philip, H. Zhi, C.-Z. Giam, NF-κB inhibition facilitates the establishment of cell lines that chronically produce human T-lymphotropic virus type 1 viral particles. *J. Virol.* **88**, 3496–3504 (2014).
61. K. H. D. Crawford *et al.*, Protocol and reagents for pseudotyping lentiviral particles with SARS-CoV-2 spike protein for neutralization assays. *Viruses* **12**, 13–15 (2020).